Check for updates

ADVANCED FUNCTIONAL MATERIALS
www.afm-journal.de

Liquid Metal Microdroplet-Initiated Ultra-Fast Polymerization of a Stimuli-Responsive Hydrogel Composite

*Jianhua Zhang, Jiahe Liao, Zemin Liu, Rongjing Zhang, and Metin Sitti**

Recent advances in composite hydrogels achieve material enhancement or specialized stimuli-responsive functionalities by pairing with a functional filler. Liquid metals (LM) offer a unique combination of chemical, electrical, and mechanical properties that show great potential in hydrogel composites. Polymerization of hydrogels with LM microdroplets as initiators is a particularly interesting phenomenon that remains in its early stage of development. In this work, an LM-hydrogel composite is introduced, in which LM microdroplets dispersed inside the hydrogel matrix have dual functions as a polymerization initiator for a polyacrylic acid-poly vinyl alcohol (PAA/PVA) network and, once polymerized, as passive inclusion to influence its material and stimuli-responsive characteristics. It is demonstrated that LM microdroplets enable ultra-fast polymerization in ≈1 min, compared to several hours by conventional polymerization techniques. The results show several mechanical enhancements to the PAA/PVA hydrogels with LM-initiated polymerization. It is found that LM ratios strongly influence stimuli-responsive behaviors in the hydrogels, including swelling and ionic bending, where higher LM ratios are found to enhance ionic actuation performance. The dual roles of LM in this composite are analyzed using the experimental characterization results. These LM-hydrogel composites, which are biocompatible, open up new opportunities in future soft robotics and biomedical applications.

1. Introduction

Recent trends in the development of hydrogels offer a wide range of material characteristics (e.g., high mechanical stretchability,[1] high electrical[2,3] and thermal conductivity[4]), multifunctionalities (e.g., actuation,[5–7] batteries,[8–10] energy harvesting,[11] and self-healing[12,13]), programmability[14] and physical intelligence.[15–17] Composite hydrogels, with fillers ranging from micro-scale (e.g., liquid metal microdroplets[13] and graphene oxide[18]) to nano-scale (e.g., carbon nanotubes[19] and silver nanowires[20]), provide the hydrogel matrices with electrical or mechanical reinforcement into their material properties beyond their intrinsic limits. In addition to material enhancement, functional fillers can also bring their specialized capabilities to the hydrogel. For instance, hydrogel composites can become magnetically responsive when dispersed with magnetic particles.[21,22] Ideally, hydrogels are embedded with a filler to provide a certain function without compromising their intrinsic properties (e.g., stretchability). In many composites, however, the fillers, which are typically rigid solids, do not always mechanically match the compliance of the soft hydrogels and hence limit their benefits. For instance, hydrogels with electrically conductive fillers above their percolation threshold often become less stretchable,[23] which is at odds with their purpose. To achieve a certain material enhancement or a unique function, pairing a hydrogel with a certain filler while minimally compromising its useful properties has been a major challenge in composite hydrogels.[15,24]

Liquid metals (LM) are excellent soft polymer fillers with their unique combination of mechanical properties (e.g., fluidic behaviors with high deformability[25] and high surface tension[26–28]) and electrical properties (e.g., high conductivity[26]). Eutectic gallium-indium (EGaIn, 75% Ga and 25% in by weight[26]) is a particularly useful liquid metal for its low melting point (15.5 °C[26]), high electrical conductivity,[26] and low toxicity.[29] When embedded into silicone elastomers, LM microdroplets enhance their mechanical properties[30–32] without significantly degrading their elasticity. With their unique combination of high electrical and thermal conductivity and low mechanical stiffness, these LM microdroplet-embedded elastomers have a wide range

J. Zhang, J. Liao, Z. Liu, R. Zhang, M. Sitti
Physical Intelligence Department
Max Planck Institute for Intelligent Systems
Heisenbergstr. 3, 70569 Stuttgart, Germany
E-mail: sitti@is.mpg.de
M. Sitti
Institute for Biomedical Engineering
ETH Zürich
8092 Zürich, Switzerland
M. Sitti
School of Medicine and College of Engineering
Koç University
Istanbul 34450, Turkey

The ORCID identification number(s) for the author(s) of this article can be found under https://doi.org/10.1002/adfm.202308238

© 2023 The Authors. Advanced Functional Materials published by Wiley-VCH GmbH. This is an open access article under the terms of the Creative Commons Attribution License, which permits use, distribution and reproduction in any medium, provided the original work is properly cited.

DOI: 10.1002/adfm.202308238

of applications, from wearable electronics to soft robotics.[25] However, compared to other polymers such as hydrogels, silicone elastomers have several limitations (e.g., low swellability, low biodegradability, inability to self-heal mechanically) that make them incompatible with some specific applications. Hydrogels offer several capabilities beyond these limits, including their ability to hydrate as well as dehydrate through their porous structure,[23] to self-heal mechanically,[33] and to conduct current through mobile ions.[6] Despite the promising potential of hydrogels, dispersing and embedding LM microdroplets remains in its early stages of development. While interfacing LM with hydrogels structurally at mm-scales has been explored in various contexts (e.g., biomonitoring electrodes[34] and 3D printing suspensions[35]), LM droplet dispersion at μm-scales similar to LM-embedded elastomers has yet to be explored in hydrogels.

Polymerization of hydrogels can influence their crosslinked structure by several factors, including the type of reaction initiator (e.g., UV, thermal, electrochemical, and persulfates) and polymerization time (typically on the order of several hours). For instance, UV-initiated photopolymerization typically takes place at a higher reaction rate than persulfate-initiated radical polymerization, which may affect crosslink density and the resulting material characteristics. Interestingly, the LM microdroplet as an unconventional polymerization initiator was recently studied for the polymerization of polyacrylamide from vinyl-based monomers,[36] where LM provides free radicals, and poly(acrylic acid) from acrylic acid monomers,[37] which can be ionically crosslinked by the gallium ions (Ga^{3+}) released from the LM microdroplets. In both cases, the hydrogel systems do not need a conventional initiator for polymerization to take place. Chemical polymerization as the primary role of LM dispersion in these systems motivates their use beyond the currently established LM microdroplet-embedded polymers, where LM microdroplets are used for their intrinsic material properties. We note that these factors are not mutually exclusive. For instance, by tuning the matrix structure through stronger crosslinks, the hydrogel may display different mechanical strengths as a result. In this sense, by their multiple roles, the inclusion of LM microdroplets may be leveraged to achieve desired hydrogel characteristics that otherwise require other compositional modifications.

Hydrogels as stimuli-responsive materials can also benefit from LM microdroplets inclusion as LM microdroplets can respond to a wide range of stimuli (e.g., electrical,[28], magnetic,[38] thermal,[39] and chemical[40]) as a passive (e.g., supporting compliant structures[41]) or active component (e.g., generating forces[27,42] or electricity[8,43]) in synergy with the hydrogels. In addition to the chemical and compositional effects of LM microdroplets at a molecular level (e.g., as polymerization initiators), their inclusion in a hydrogel matrix also has interfacial and functional consequences at a structural level (e.g., LM microdroplets may influence the hydrogel's ability to absorb water). This multilevel duality further exploits the role of LM microdroplets in a stimuli-responsive hydrogel beyond their conventional uses.

This study presents an LM microdroplets-hydrogel composite in which LM microdroplets have dual functions as a polymerization initiator for a poly(acrylic acid)–poly(vinyl alcohol) (PAA/PVA) network and, once polymerized, as passive inclusion to influence the hydrogel functionalities (**Figure 1**A). We highlight the remarkably reduced polymerization time by using LM microdroplets as a controllable initiator (≈1 min) in this work. Compared to existing polymerization methods the LM-initiated polymerization is remarkably faster (1 min vs several hours) at a similar range of molar concentrations of the initiator (e.g., LM: $\approx 10^{-1}$ mol L^{-1} compared to persulfates: $\approx 10^{-2} - 10^{-1}$ mol L^{-1}, Figure 1B). This LM microdroplet-initiated ultra-fast polymerization technique also affects the responsiveness of hydrogel to electrical stimuli. The LM-hydrogel composite results in higher stimuli responsivities of the hydrogels when used as an electrical bending actuator. We show that LM microdroplet-hydrogel thin films bend faster ionically in an electric field compared to similar work, with higher LM ratios resulting in higher bending speeds (Figure 1B). To investigate the ultra-fast polymerization mechanism, we analyzed the rheological behaviors of AA monomer, AA-PVA solution, and LM-AA-PVA hydrogel during the crosslinking process. The mechanical performance of the LM microdroplet-hydrogel over various dehydration stages (i.e., a soft stage, followed by a tough stage after 24 h and eventually a rigid stage, Figure 1C) is characterized. We demonstrate that LM microdroplets significantly enhance the maximum strain of the rigid LM microdroplets-crosslinked PAA/PVA hydrogel by ≈10 times compared to the LM-free, UV-crosslinked PAA/PVA hydrogel after swelling. As a stimuli-responsive material, we examine the LM microdroplet-tunable bending ability of the LM microdroplet-hydrogels in response to electric fields by osmosis and humidity by swelling. These behaviors are further demonstrated in self-folding structures and controllable robot locomotion. Finally, we discuss the biocompatibility of the LM microdroplet-hydrogel composites and propose future prospects for the dual roles of LM in hydrogel polymerization and functionalities.

2. Results and Discussion

2.1. LM-Hydrogel Composites

2.1.1. Characteristics of the LM-Hydrogel Composites

To fabricate the LM microdroplets-hydrogel composites, polyvinyl alcohol (PVA) powder was dissolved in a solution of acrylic acid (AA) and phosphate-buffered saline (PBS) to obtain a homogeneous solution. LM (eutectic Ga 75% and In 25% by weight) was added in four various quantities (0, 100, 200, and 300 mg), which were labeled hereinafter as LM-0, LM-100, LM-200, and LM-300 groups. The LM microdroplet initiated the polymerization of AA monomers through rapid radical polymerization, facilitated by sonication of the LM droplets for 1 min. The stable colloidal suspension of LM droplets was produced with a broad diameter range from $\approx 10^{-8}$ to $\approx 10^{-6}$ m and incorporated into the polymer network (Figure 1A,F; Figure S2, Supporting Information). It was observed that homogeneity of the LM microdroplets began to degrade as the LM content exceeded 400 mg, where millidroplets visibly appeared (Figure S3D, Supporting Information). This inherent limit on the LM content can be explained by the polymerization duration, where a larger volume of LM requires a longer time for sonication than polymerization. This sonication process produced smaller LM droplets, increased total surface area, and accelerated the formation of PAA-PVA hydrogel.

© 2023 The Authors. Advanced Functional Materials published by Wiley-VCH GmbH

16163028, 0, Downloaded from https://onlinelibrary.wiley.com/doi/10.1002/adfm.202308238 by Koc University, Wiley Online Library on [26/02/2024]. See the Terms and Conditions (https://onlinelibrary.wiley.com/terms-and-conditions) on Wiley Online Library for rules of use; OA articles are governed by the applicable Creative Commons License

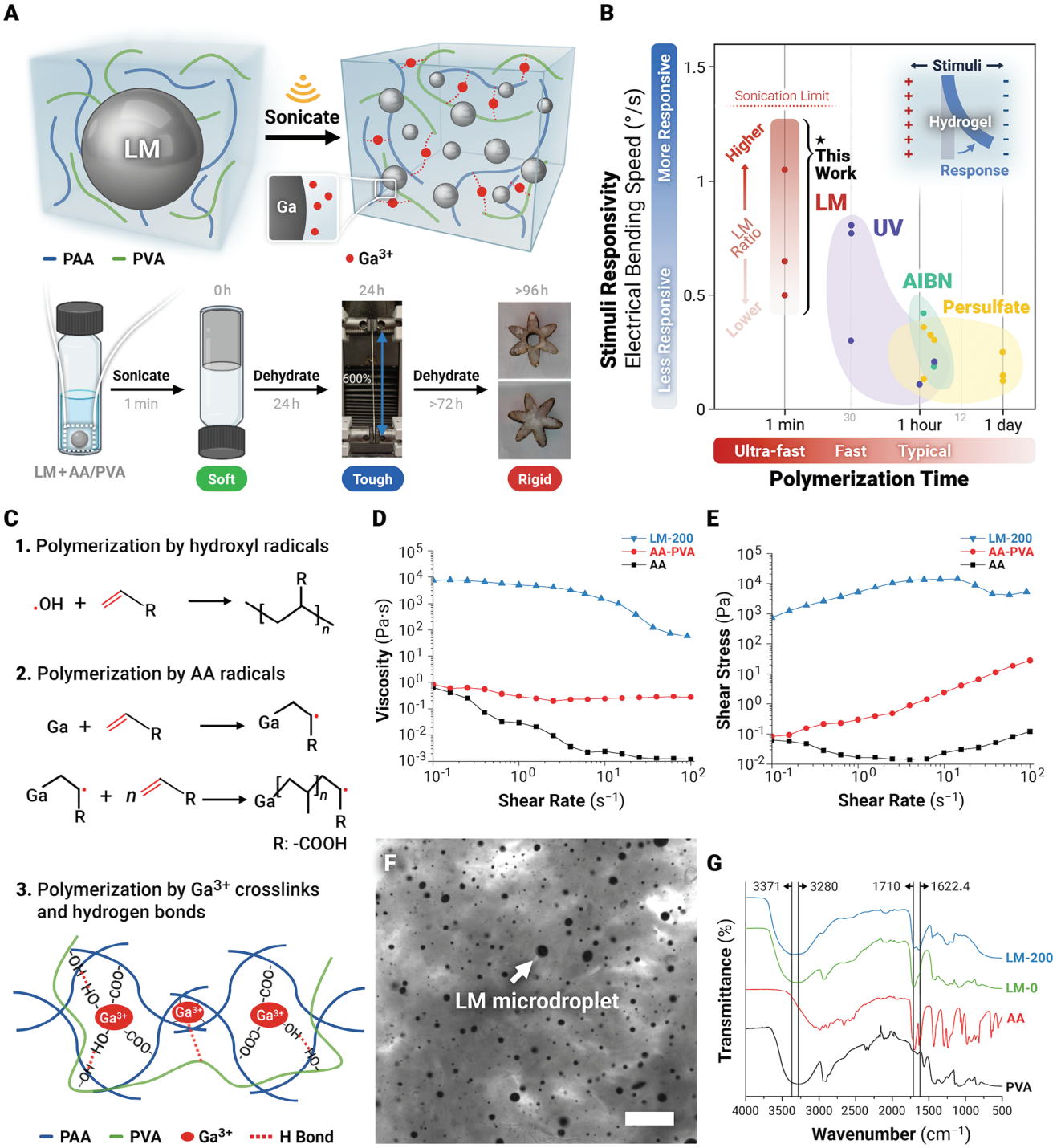


Figure 1. Polymerization mechanisms of the liquid metal (LM) microdroplet-hydrogel composite. A) (Top) Sonication of liquid metal into microdroplets enables ultra-fast, LM-initiated polymerization (1 min) of the LM-PAA-PVA hydrogel. (Bottom) The resulting hydrogels transition from a soft to a tough and eventually rigid state through dehydration at room temperature. B) Compared to existing polymerization methods,[44–56] the LM-initiated polymerization is remarkably faster (1 min vs several hours) at a similar range of molar concentrations of the initiator (e.g., LM: $\approx 10^{-1}$ mol L^{-1} compared to persulfates: $\approx 10^{-2} - 10^{-1}$ mol L^{-1}). The LM polymerization also results in higher stimuli responsivities of the hydrogels when used as an electrical bending actuator. C) The polymerization of the LM-PAA-PVA hydrogel involves hydroxyl radicals, acrylic acid radicals, Ga^{3+} cross-links, and hydrogen bonds. Rheological characterization was performed on the acrylic acid (AA) monomer, AA-PVA solution, and LM-200 soft hydrogel after sonication, viscosity (D), and shear stress (E). F) Morphology and distribution of the LM microdroplets in the LM-200 soft hydrogel. (Scale bar: 10 μm). G) FTIR spectra of PVA, AA monomer, the LM-0, and LM-200 groups.

© 2023 The Authors. Advanced Functional Materials published by Wiley-VCH GmbH

16163028, 0, Downloaded from https://onlinelibrary.wiley.com/doi/10.1002/adfm.202308238 by Koc University, Wiley Online Library on [26/02/2024]. See the Terms and Conditions (https://onlinelibrary.wiley.com/terms-and-conditions) on Wiley Online Library for rules of use; OA articles are governed by the applicable Creative Commons License

The pre-gel solution underwent a "sol–gel" transition and transformed into a soft hydrogel. The soft hydrogel exhibited remarkable mechanical strengths such as high stretchability, with a maximum strain of up to ≈2500% (Figure S1A1, A2, Supporting Information), as well as self-healing capabilities, where the polymeric network was able to completely recover after dissection and recontact (Figure S1B, Supporting Information). The conductivity of the LM-200 group was $10.3 \pm 1.4 \times 10^{-3}$ S m^{-1}, which was higher than that of the LM-0 group ($2.3 \pm 0.2 \times 10^{-3}$ S m^{-1}). Moreover, the conductivity remained consistent before and after healing in the LM-200 group. The higher conductivity may be attributed to the presence of LM microdroplets.[57] By leveraging the self-healing capability, hydrogels with different LM concentrations were able to be combined through self-healing while maintaining high stretchability (Figure S1D, Supporting Information). The soft LM-hydrogel was molded into a thin sheet (thickness: 1 mm) and dehydrated for 24 h, which transitioned the hydrogel into a tough stage, with gradually improving mechanical toughness. During this process, the LM-hydrogel became less stretchable (maximum strain decreased from 600% to 300%). Finally, the LM-hydrogel became completely dehydrated and rigid, where it became the least stretchable (<20% maximum strain after 96 h). One benefit of dehydration was to facilitate laser-cutting of the rigid polymer into the desired shapes.

2.1.2. Mechanisms of LM-Initiated Ultra-Fast Polymerization

The polymerization reactions of acrylic acid (AA), which is conventionally initiated by free radicals from certain initiators (e.g., ammonium persulfate or potassium persulfate), is recently found to be achievable with Ga-based liquid metals[36,37] through two distinct mechanisms. First, Ga is used as a source of free radicals due to its atomic configuration with one unpaired electron,[36,58] which gives Ga the tendency to release radicals to initiate the polymerization reactions. Second, Ga^{3+} ions released from Ga surfaces can function as ionic crosslinkers in some systems.[59] Our study presents an ultra-fast polymerization method where Ga, in its eutectic form with In as a liquid metal, is sonicated for greater surface areas. The exposed Ga and Ga^{3+} ions then initiated co-polymerization of PAA and PVA by these two concurring mechanisms of radical and ionically crosslinking (Figure 1C). While a longer sonication time can increase Ga surface area[60] and expose the system to a larger number of Ga^{3+} ions and hence denser crosslinking, we note that the formation of the crosslinks may also prevent breaking up the LM droplets further after a certain time limit. In addition to the LM contribution to ultra-fast polymerization, we also observe distinct rheological trends between AA-PVA and AA monomer solutions (i.e., higher viscosities and shear stresses in the former; Figure S1D,E, Supporting Information), which is consistent with the known effects of rheology on polymerization kinetics.[61,62] The rapid increase in the viscosity of AA-PVA system also agrees with the strong molecular interactions due to the hydroxyl groups in PVA.

As summarized in Figure 1C, we identify three types of crosslinks that account for the polymerization of the LM microdroplets-PAA-PVA system. First, radicals can be provided by the hydroxyl groups in oxygen, water, and PVA solutions during the sonication process. Second, AA can also release radicals to participate in polymerization. Third, the LM can release Ga^{3+} and can form ionic crosslinks with −COO− in the PAA system. To study the effect of LM ratios, we tested the LM-hydrogels in three different groups, namely LM-100, LM-200, and LM-300 and compared them to a control group of LM-free PVA/PAA (LM-0) that was UV-crosslinked. Once polymerized, the LM microdroplets are immobilized in the hydrogel network (Figure 1F; and Figure S3A–C, Supporting Information). The complexation was confirmed by enhanced FTIR absorption of −COO− at 1622.4 cm^{-1} (Figure 4D). Furthermore, FTIR spectroscopy confirmed the surface interaction between LM and PVA. While the characteristic peak for the stretching vibration of the –OH group is typically observed at 3280 cm^{-1}, a shift of 90 cm^{-1} was observed in the case of LM-PAA-PVA, indicating the presence of hydrogen bonding between LM microdroplets and PVA chains. Rheological analysis revealed that the loss modulus (G'') became close to the storage modulus (G') and the low tangent ($\tan\delta = G''/G'$) was ≈1, indicating the formation of weak hydrogels with a low crosslink density in the soft stage. In the low frequency regime, G'' exceeded G' and exhibits liquid-like behaviors, whereas in the high frequency regime, G' surpassed G'' and started to show solid-like behaviors (Figure S4A–C, Supporting Information), which is consistent with the behaviors found in previous work on LM-sonication-based polymerization of AA monomers.[37]

Overall, the ultra-fast polymerization method demonstrated in this work marks a distinct regime in terms of LM microdroplet-initiated PAA-PVA polymerization kinetics (≈1 min compared to several hours, Figure 1B) and LM microdroplet-enabled multiple crosslinking mechanisms (Figure 1C) that complement conventional polymerization methods for hydrogels.

2.2. Stage Transition of the LM-Hydrogels

2.2.1. Hydrogel Transition from the Soft to Tough Stages

We define the characteristic stages based on the mechanical and rheological properties of the LM-hydrogel composite, where the soft hydrogel transitions into the tough hydrogel stage after 24 h of gelation. The storage modulus (G') significantly increased and exhibited angular frequency-independent plateaus, while the tangent delta ($\tan\delta$) remained < 1 across the entire frequency range of 0.1–100 rad s^{-1}, indicating the formation of a robust gel network with a high crosslink density. **Figure 2**C shows the results of the oscillation rheology tests to investigate the evolution in mechanical properties after 24 h of gelation. Strain sweeps with an applied strain of 1–100% showed no critical point, indicating the absence of phase separation. This soft-tough transition is consistent with previous work on LM-polymerized PAA hydrogels,[37] which toughen after 24 h.

2.2.2. Self-Healing Ability of the Tough LM-Hydrogel

The LM-hydrogel system exhibited self-healing ability without the need for additives such as water or acid after 24 h. Figure 2D illustrates a dog-bone-shaped LM-hydrogel sample

© 2023 The Authors. Advanced Functional Materials published by Wiley-VCH GmbH

16163028, 0, Downloaded from https://onlinelibrary.wiley.com/doi/10.1002/adfm.202308238 by Koc University, Wiley Online Library on [26/02/2024]. See the Terms and Conditions (https://onlinelibrary.wiley.com/terms-and-conditions) on Wiley Online Library for rules of use; OA articles are governed by the applicable Creative Commons License

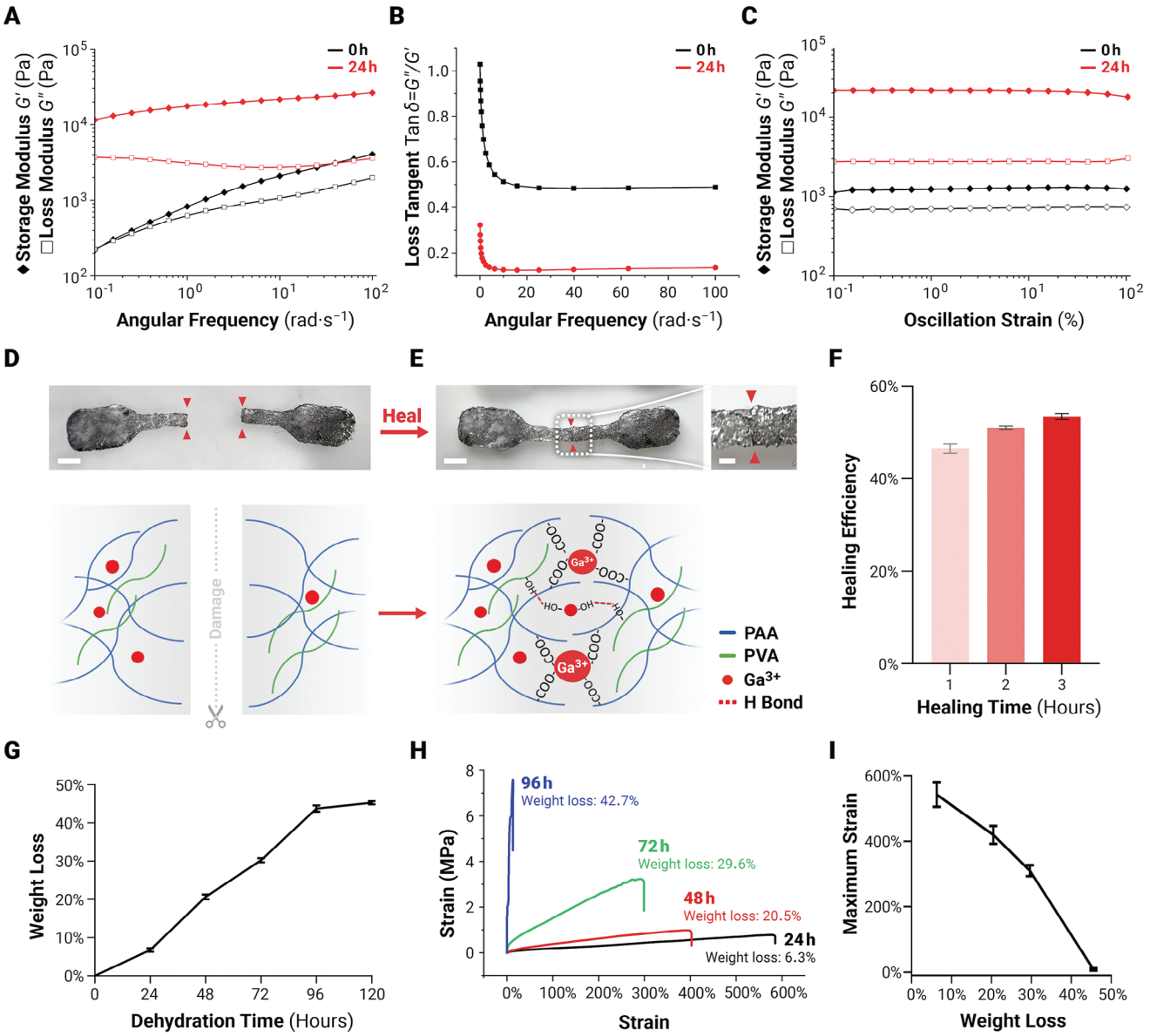


Figure 2. Stage transition and self-healing ability of the LM-hydrogel . Rheological characterization was performed on the LM-200 group after sonication (0 h) and at the tough stage (24 h): A) Frequency sweeps, B) loss tangent, and C) strain sweeps. D) Principles of LM-initiated self-healing in hydrogels, where further Ga^{3+} ions and H bonds form between the two cut LM-hydrogel sections. E) A schematic diagram illustrates the self-healing property of the LM tough composite hydrogels, which is attributed to the hydrogen bond formation and the release of Ga^{3+} ions from the liquid metal particles. Scale bar: 3 mm. F) The healing efficiency of the LM-200 group was assessed after cutting for 1, 2, and 3 h. G) The weight loss of the LM-200 group was monitored over time. H) The stress–strain relationship of the LM-200 group was evaluated at different time points (24, 48, 72, and 96 h) to investigate the evolution of its mechanical properties over time. I) The relationship between weight loss and maximum strain was analyzed to explore the correlation between these two factors in the LM-200 group.

cut into two halves and then merged by pressing for 1 min. Figure S3F–H(Supporting Information), shows the stress–strain curves for the LM-0, LM-100, LM-200, and LM-300 groups before and after the healing process. Notably, the LM-hydrogel groups (LM-100, LM-200, and LM-300) display greater strain compared to the LM-0 group prior to cutting. The strain, however, decreases slightly at higher LM concentrations, which can be explained by the occupation of the hydrogel network by the increasing number of LM droplets. After 3 h of healing after cuts, the LM-hydrogel groups show remarkable self-healing efficiencies of over 50% compared to 0% in the LM-0 group. This self-healing process was facilitated by two mechanisms: First, the presence of LM, which can release Ga^{3+} during hydrogel deformation and rupture under acidic conditions. The ionic interconnections between –COO– of PAA and Ga^{3+} promote healing. Second, hydrogen bonding interactions form between LM, water, and PVA. These hydrogen bonds contribute to healing. The healing efficiency of the tough hydrogel was 45% after 1 h of cutting, and

© 2023 The Authors. Advanced Functional Materials published by Wiley-VCH GmbH

16163028, 0, Downloaded from https://onlinelibrary.wiley.com/doi/10.1002/adfm.202308238 by Koc University, Wiley Online Library on [26/02/2024]. See the Terms and Conditions (https://onlinelibrary.wiley.com/terms-and-conditions) on Wiley Online Library for rules of use; OA articles are governed by the applicable Creative Commons License

16163028, 0, Downloaded from https://onlinelibrary.wiley.com/doi/10.1002/adfm.202308238 by Koc University, Wiley Online Library on [26/02/2024]. See the Terms and Conditions (https://onlinelibrary.wiley.com/terms-and-conditions) on Wiley Online Library for rules of use; OA articles are governed by the applicable Creative Commons License

it increased over 3 h due to a sustained Ga^{3+} release and hydrogen bond formation. We also note that self-healing efficiencies are enhanced by higher LM contents for the increasing release of Ga^{3+} ions. Similar healing efficiency trends have been observed in LMs@rGO/PAA samples within the initial few hours (2–10 h),[59] and the coordination bonding rate decreases once Ga^{3+} diffusion reaches equilibrium. Figure 2F and Figure S3H, Supporting Information, show that self-healing efficiency increases with a longer healing time and higher LM concentrations. This phenomenon can be attributed to enhanced hydrogen bonding and interactions between Ga^{3+} and $-COO^-$ group. The self-healing capability of the stretchable LM-hydrogel composite can benefit soft robotic devices for continual operation after significant mechanical damage.[63] Meanwhile, various LM concentrations could be combined into a single sample, due to the self-healing capabilities of the LM-hydrogel composite. However, the strain observed in the healing sample (LM-100-200-300) was lower compared to the LM-100, LM-200, and LM-300 groups (Figure S3G, Supporting Information).

2.2.3. Hydrogel Transition from the Tough to Rigid Stages

Due to the presence of PBS solution in our hydrogel system, we further investigated dynamic mechanical properties of the hydrogel over the dehydration process. As shown in Figure 2G and Figure S3E, Supporting Information, weight loss of the LM-hydrogel increased over time until most water evaporated. The water content underwent a significant reduction within 96 h, reaching nearly 0% by the 120-h mark. This observation suggests that the LM hydrogel composite had transformed into a fully dried polymer at the 120-h mark. Tensile experiments demonstrated increasing mechanical properties in the dehydration process (Figure 2H), indicating the formation of a higher crosslink density and more robust gel networks during the transition. However, the maximum strain decreased from ≈600% to ≈300% from 24 to 72 h. The maximum strain drastically declined from 72 to 96 h and the weight loss increased from 29.3% to 42.7%. Interestingly, the maximum strain was found to decrease and exhibit an inverse correlation with weight loss (Figure 2I).

2.3. Effect of LM Microdroplets on Swelling and Bending

The ability to absorb and contain water through the porous hydrogel matrix is highly influenced by its structural (e.g., pore size distribution,[64] porosity,[65] and specific surface area[66]) and interfacial characteristics (e.g., contact angle[67]). In this work, we analyze the effect of using LM microdroplets as a polymerization initiator[36,59] and a passive inclusion to the PAA-PVA hydrogel on its water uptake behaviors over time. This method of LM-initiated polymerization is demonstrated here as a means of tuning the swellability of a hydrogel, which can be used in applications that require programmable swelling-enabled bending motions.

2.3.1. Swelling Characterization and Theory

For characterization, we synthesized rectangular films of LM-hydrogels with different LM ratios by mixing LM content (0, 100, 200, and 300 mg, denoted LM-0, LM-100, LM-200, and LM-300, respectively) with the PAA-PVA gel. Prior to the swelling experiment, the mechanical properties of the rigid LM hydrogel composites were investigated. As shown in Figure S5A,B, Supporting Information, all those hydrogels had very low strain (<10%) in tensile experiments, while the elastic modulus was around 500 MPa. Meanwhile, SEM microscopy was used to visualize the surface morphology of the rigid LM hydrogel composites, as shown in Figure S6, Supporting Information. LM-0 had a smooth surface, while LM microdroplets were trapped on the surfaces of LM-100, LM-200, and LM-300 groups. More LM microdroplets were observed with higher LM concentration groups. The rigid LM hydrogel composites were submerged in water, and swelling ratios were tracked over time (i.e., weight expansion $\frac{W_t - W_0}{W_0}$, where W_t is the hydrogel weight after swelling at t h and W_0 is the initial dry weight) over 7 days (**Figure 3**C,D). In terms of macroscopic expansion due to water uptake, the LM-hydrogels (LM-100, LM-200, and LM-300) displayed higher equilibrium uptake W_∞ compared to the non-LM-hydrogel (LM-0), which suggests higher porosities that were contributed by the structural effect of LM on crosslinking (Figure 3B). LM-0 had a compact hydrogel structure, whereas the LM-PAA-PVA groups showed porous structures after swelling and freeze-drying (Figure S7, Supporting Information). Within the groups of LM-hydrogels, we observed a trend of lowering W_∞ as LM content increased, from which we inferred that the presence of LM affects water uptake in more than one competing mechanism as follows.

LM for Wettability (Higher Water Uptake with Higher LM Contents): By this hypothesis, the LM microdroplets embedded in the hydrogel matrix provide an abundant surface gallium oxide that is highly hydrophilic (near-zero contact angle of water[68,69]), which agrees with lower water uptakes in the LM-0 hydrogels. In other words, LM microdroplets may enhance local wettability ϕ in the capillary structure and hence contribute positively to the overall diffusivity. To see this, consider a hypothetical small capillary cross-section (radius r, length L considering a tubular equivalent to a pore[70]) that is assumed to be surrounded by LM only (i.e., in the LM-hydrogels) as opposed to gel crosslinks only (i.e., in the non-LM-hydrogels). The time t required for this small section to fully absorb water can be solved from the Lucas–Washburn equation[71–73] as

$$t = \left(\frac{1}{\cos\phi}\right)\left(\frac{2\eta L^2}{\gamma r}\right) \tag{1}$$

where ϕ is the water contact angle (in this case ≈0° with LM and ≫0° without LM), η is the dynamic viscosity of water, and γ is the surface tension of water. Note that we only consider water intake in an infinitesimally small tube and neglect the elastic expansion of the wall. Clearly, this mechanism favors the presence of LM for a shorter period of t required to fill the tube.

This LM surface theory, however, does not solely contribute to the overall swelling behavior due to a simple scaling law: More LM microdroplets would have multiplied the number of such hypothetical capillary tubes, which does not explain the general trend of decreasing water uptake with higher LM ratios (Figure 3D). This suggests a second mechanism at play in the LM-embedded regime.

© 2023 The Authors. Advanced Functional Materials published by Wiley-VCH GmbH

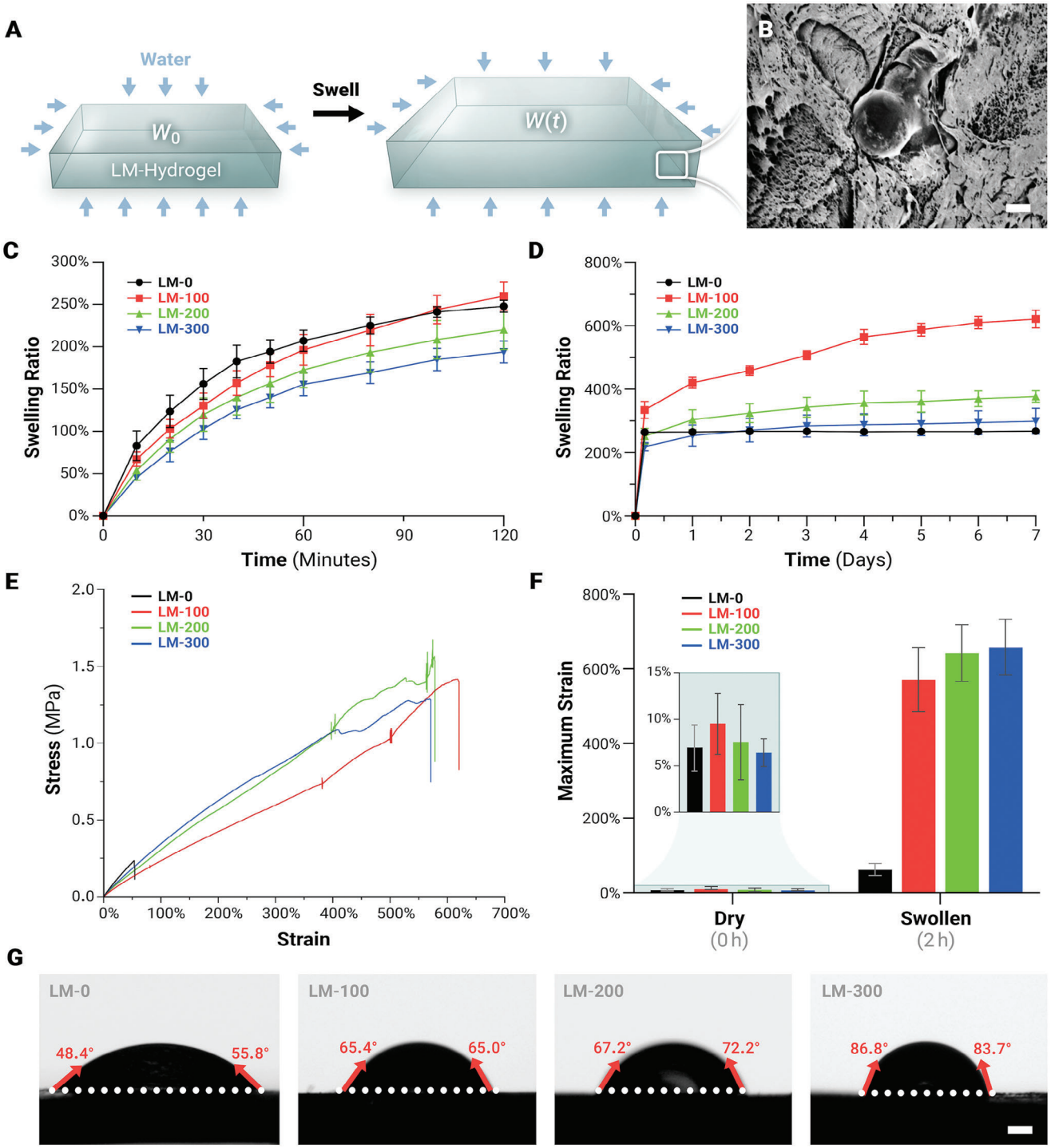


Figure 3. Effects of LM inclusion on hydrogel swelling. A) A thin film of LM-hydrogel is placed in a water bath and functions as a porous medium for water (left). Driven by the capillary actions across the hydrogel surface, the water uptake into the hydrogel matrix enlarges the volume (right). B) A representative SEM image of an LM-100 sample showing the inclusion of LM microdroplets after swelling and freezer drying, scale bar 2 µm. C) Hydrogel swelling ratio in the first ≈120 min displays a monotonic relationship between LM ratios and water uptake (i.e., LM-0 absorbs the fastest). After ≈120 min, this relationship transitions into a new regime (i.e., LM-0 absorbs the slowest). A trend is observed among the LM hydrogels, where higher LM contents cause lower swelling capacity, a phenomenon in agreement with our theoretical analysis. D) Equilibrium water uptake after 7 days shows that the second regime stabilizes. E) The stress–strain curves of the LM composite rigid hydrogel after swelling for 2 h. F) Maximum strain changes before swelling (rigid) and after 2 h swelling in water. G) The water contact angle on the LM-hydrogels contributes to the microscopic capillary water uptake and overall swelling behavior, water volume 50 µL.

© 2023 The Authors. Advanced Functional Materials published by Wiley-VCH GmbH

16163028, 0, Downloaded from https://onlinelibrary.wiley.com/doi/10.1002/adfm.202308238 by Koc University, Wiley Online Library on [26/02/2024]. See the Terms and Conditions (https://onlinelibrary.wiley.com/terms-and-conditions) on Wiley Online Library for rules of use; OA articles are governed by the applicable Creative Commons License

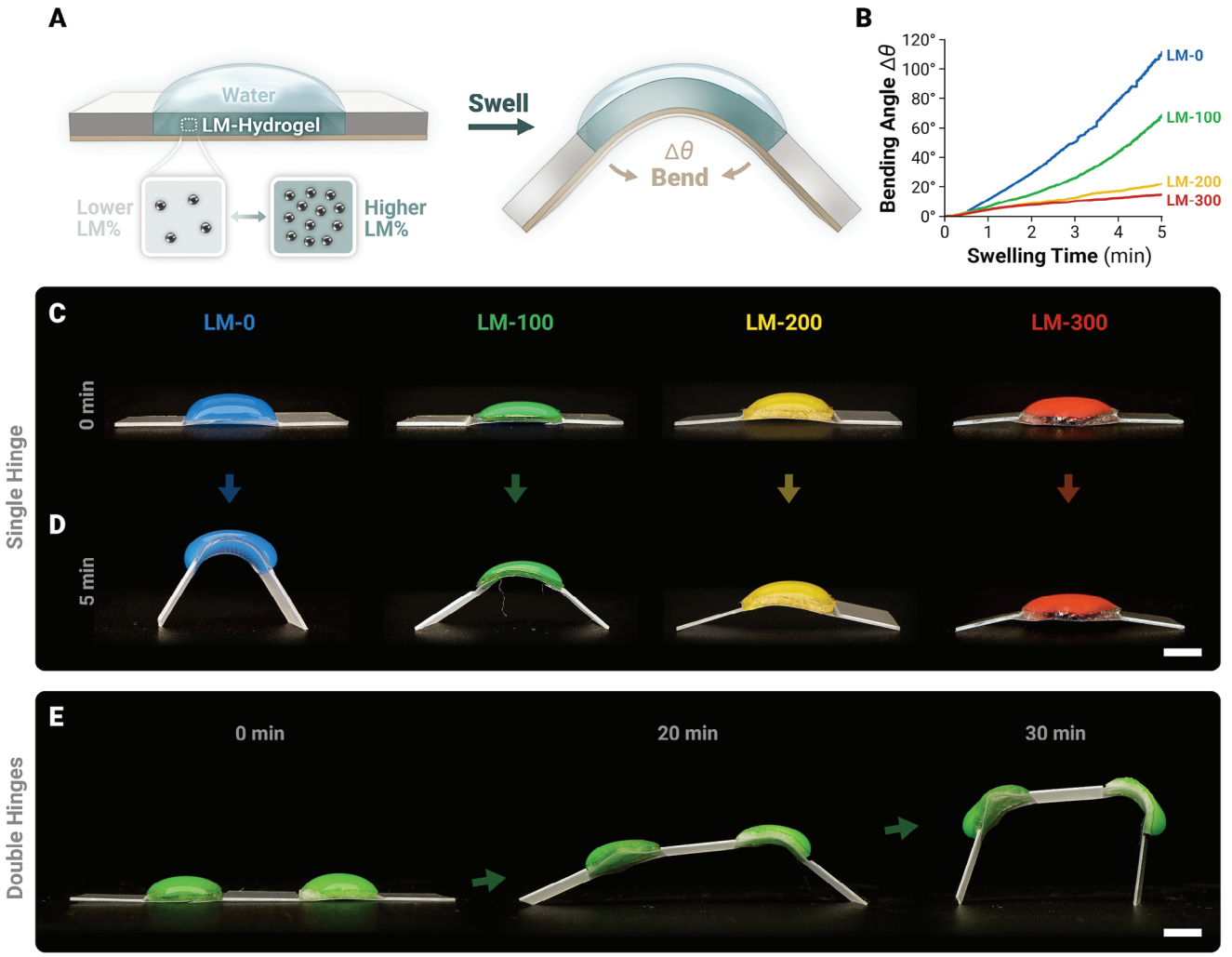


Figure 4. Effects of LM microdroplets on hydrogel bending by constrained swelling. A) An elastically hinged structure is made from a thin film of LM-hydrogel taped on the bottom side along with two rigid plates of transparency films (left). Upon swelling on the top side due to a droplet of water, the hinge expands on the top, whereas the bottom face is constrained, resulting in an overall bending (right). B) The swelling-induced bending behavior in four LM-hydrogel samples with different LM ratios, where higher LM content generally lowers the bending speed and the final angle as a result. C,D) Actual images of bending of the LM-hydrogel samples at 0 min (C) and 5 min (D), which can be used as a building block for more sophisticated self-folding structures with programmable folding behaviors in each hinge, scale bar 2 mm. E) A more complex self-folding structure with double LM-hydrogel hinges. After 30 min of swelling, a 2D linked structure transforms into a 3D table-like geometry in response to bending in both hinges. Scale bar 2 mm.

LM for Polymerization (Lower Water Uptake with Higher LM Contents): Structural effect on the LM-initiated crosslinks, as previously analyzed, is found to be more significant with higher LM contents.[36] Pore sizes r are generally considered to be smaller with stronger crosslinks,[64] which in this work is found to be related to the presence of LM microparticles, which may contribute to the inhibition of water uptake by the Lucas–Washburn equation (Equation (1)) where $t \propto r^{-1}$ as opposed to $t \propto \sec\phi$ in the first mechanism. Furthermore, interfacial characterization of water contact angle ϕ on the non-LM-hydrogel and LM-hydrogels (Figure 3G) also reveals increasing ϕ as LM contents increase, which by the same equation also contributes to the lowering water uptake.

Swelling is therefore theorized to be less significant when there are more LM microdroplets scattered across the hydrogel matrix, which would decrease microscopic capillary perimeters and hence macroscopic swelling capacity. We also note that it is unlikely that the dual mechanisms proposed here can be sufficiently described solely by a classic first-order swelling kinetics by Fick's laws[65]

$$\ln\left(\frac{W_\infty}{W_\infty - W(t)}\right) \approx \frac{\pi^2 Dt}{h^2} \quad (2)$$

The presence of LM microparticles, by the analysis here, may contribute to the non-Fickian transport of water through the hydrogel matrix. Overall, the inclusion of LM microparticles as both polymerization initiators and passive hydrophilic components creates a new class of porous media where swelling rate and

© 2023 The Authors. Advanced Functional Materials published by Wiley-VCH GmbH

16163028, 0, Downloaded from https://onlinelibrary.wiley.com/doi/10.1002/adfm.202308238 by Koc University, Wiley Online Library on [26/02/2024]. See the Terms and Conditions (https://onlinelibrary.wiley.com/terms-and-conditions) on Wiley Online Library for rules of use; OA articles are governed by the applicable Creative Commons License

capacity are governed by multiple roles of LM that influence polymeric structure[36] and local wettability.[69,74]

The coupling of the two mechanisms proposed above also displays time dependence, where the non-LM-hydrogel swells faster than the LM-hydrogels within the first hour (Figure 3C) and slows down after the first hour. The exact mechanism of this transition, where one of the above mechanisms overtakes the other, is unknown. In terms of the tunability of hydrogel swellability, this transition marks two distinct regimes, where swelling occurs faster monotonically with LM contents in the first regime and a more complex LM-dependence in the second regime toward equilibrium ($t \to \infty$). It is unknown how drying behavior differentiates among different LM ratios over time once the LM-hydrogels are removed from an aqueous environment. Meanwhile, the mechanical properties of the LM hydrogel composites after swelling were also investigated. As shown in Figure 3E,F, and Figure S5C,D, Supporting Information, LM-0 had a very small strain change (≈50%) compared to the rigid hydrogel (≈8%), which showed a brittle property. However, the maximum strain of the LM-hydrogel groups was around 600%, which was significantly increased from the rigid hydrogel (≈8%). Compared to LM-0 hydrogel, LM-100, LM-200, and LM-300 hydrogels showed tough hydrogel properties with good stretchability. Overall, swelling behaviors in the LM-hydrogel are considered influenced by the inclusion of LM microdroplets in more than one competing mechanism. Dynamic transitions of these influences are also observed over time. Different swelling behaviors and crosslinking methods also affect mechanical properties.

2.3.2. Influence of LM Microdroplets on Bending Hydrogel by Constrained Swelling

Hydrogel swelling allows for a variety of programmable motions that are not limited to the omnidirectional volume expansion (**Figure 4**A) but rather many possible constrained motions[75] that arise from asymmetric expansion and shrinking in the hydrogel (Figure 4A,B). One typical example is bending in a thin film, which occurs under one or both of the conditions. First, the hydrogel may generate overall bending by absorbing water faster on one side than the other.[76] Second, the hydrogel may bend by integrating a kinematic constraint on one side as a strain limiter such that any volume expansion only affects the non-constrained side. Here, we demonstrate a bending design that enables both conditions by taping one side of a LM-hydrogel film (length: 8.5 mm, depth: 5.5 mm, thickness: 0.85 mm; all in the dehydrated state) to two rigid transparency films (length: 7.5 mm, depth: 5.5 mm, thickness: 0.5 mm). This configuration allows the LM-hydrogel to act as an elastic hinge that connects the two rigid films, similar to classic self-folding structures.[77–79] We created the bending LM-hydrogel with different LM ratios (LM-0, LM-100, LM-200, and LM-300). With an initial configuration where the hinge was flattened, we covered the LM-hydrogel with a dyed water drop and allowed it to be absorbed by the LM-hydrogel overtime. We recorded the bending motion on a camera for accurate video analysis. The water drop was dyed in different colors for different LM-hydrogel samples, where the effect of dyes on water absorption is assumed to be negligible, to visually mark the difference between the LM ratios.

The results after 5 min showed that the change in bending angle of LM-0 was the highest (111.3°) and followed by LM-100 (68.4°), LM-200 (21.9°), and LM-300 (14.8°) (**Figure 5**; Video S1, Supporting Information). We calculated the radial stresses at the tip of the beam for the LM-0/100/200/300 groups as 145.31, 37.32, 19.70, and 14.10 kPa, respectively, which is consistent with the observation that higher LM ratios degrade swellability of the LM-hydrogels. This trend is in decent agreement with the swelling characterization (Figure 4C,D) and the theoretical analysis above, as this swelling time is still in the first regime before the transition. We note that, in this configuration, we assume that the LM-hydrogel only absorbs water from its top surface, and hence the effect due to the weight of the water drop is symmetric.

To demonstrate a more complex self-folding capability, we designed a doubly hinged structure that consists of two hydrogel films and three rigid plates (Figure 4F). This structure began in a 2D configuration, with all the plates horizontally aligned, and was folded into 3D by swelling each hydrogel hinge for 30 min (Figure 4E; Video S2, Supporting Information). This multi-hinge configuration allows for higher degrees of freedom in programming the shape transformation by differentiating the swelling behaviors in the LM-hydrogel hinges. For instance, as demonstrated in Figure 4E, hinges made with the same LM ratio are expected to fold at nearly the same speed and result in a nearly symmetric shape upon deployment. By varying LM ratios in the hinges, the structure can be, in theory, programmed to fold into a variety of 3D geometries[77,80] with their desired curves and surfaces encoded into the LM ratios in the hydrogels. In addition to conventional single-stage folding, the LM-varying method in this work can also potentially apply to sequential folding[81] where the structure goes through multiple folding stages according to the LM ratios. In summary, spatial and temporal programmability can be potentially achieved by controlling the LM ratios in the hydrogel hinges.

2.4. Ionic Mobility and Electrical Actuation

2.4.1. Ionic Mobility and Osmotic Pressure

The ability to convert electrical energy into useful mechanical work in the case of ion-carrying polymers such as conjugated ionic conductive polymers,[82] ionic polymer-metal composites (IPMC)[83,84] and ionic hydrogels,[85] is typically a result of water migration in response to an electric field (Figure 5A). In the case of hydrogel thin films, whose shapes are determined by the balance of local water content, electric stimuli are typically used to ionically alter the balance. This electrically responsive effect is reliant on physical asymmetry across the ionizable hydrogel, in which anions (e.g., COO^- in our PAA/PVA system) are immobilized by the crosslinked matrix while cations (e.g., Na^+ in PBS solution) can move freely. When osmotic pressure across the hydrogel ($\Delta\Pi$, Figure 5A) becomes imbalanced ($\Delta\Pi > 0$) under an electric field (strength: E), the hydrogel becomes more hydrated on the anode side than the cathode side and curves toward the cathode as a result (Figure 5A).

We theoretically analyzed this ionic bending behavior (Section S2, Supporting Information) in terms of ion mobility

© 2023 The Authors. Advanced Functional Materials published by Wiley-VCH GmbH

16163028, 0, Downloaded from https://onlinelibrary.wiley.com/doi/10.1002/adfm.202308238 by Koc University, Wiley Online Library on [26/02/2024]. See the Terms and Conditions (https://onlinelibrary.wiley.com/terms-and-conditions) on Wiley Online Library for rules of use; OA articles are governed by the applicable Creative Commons License

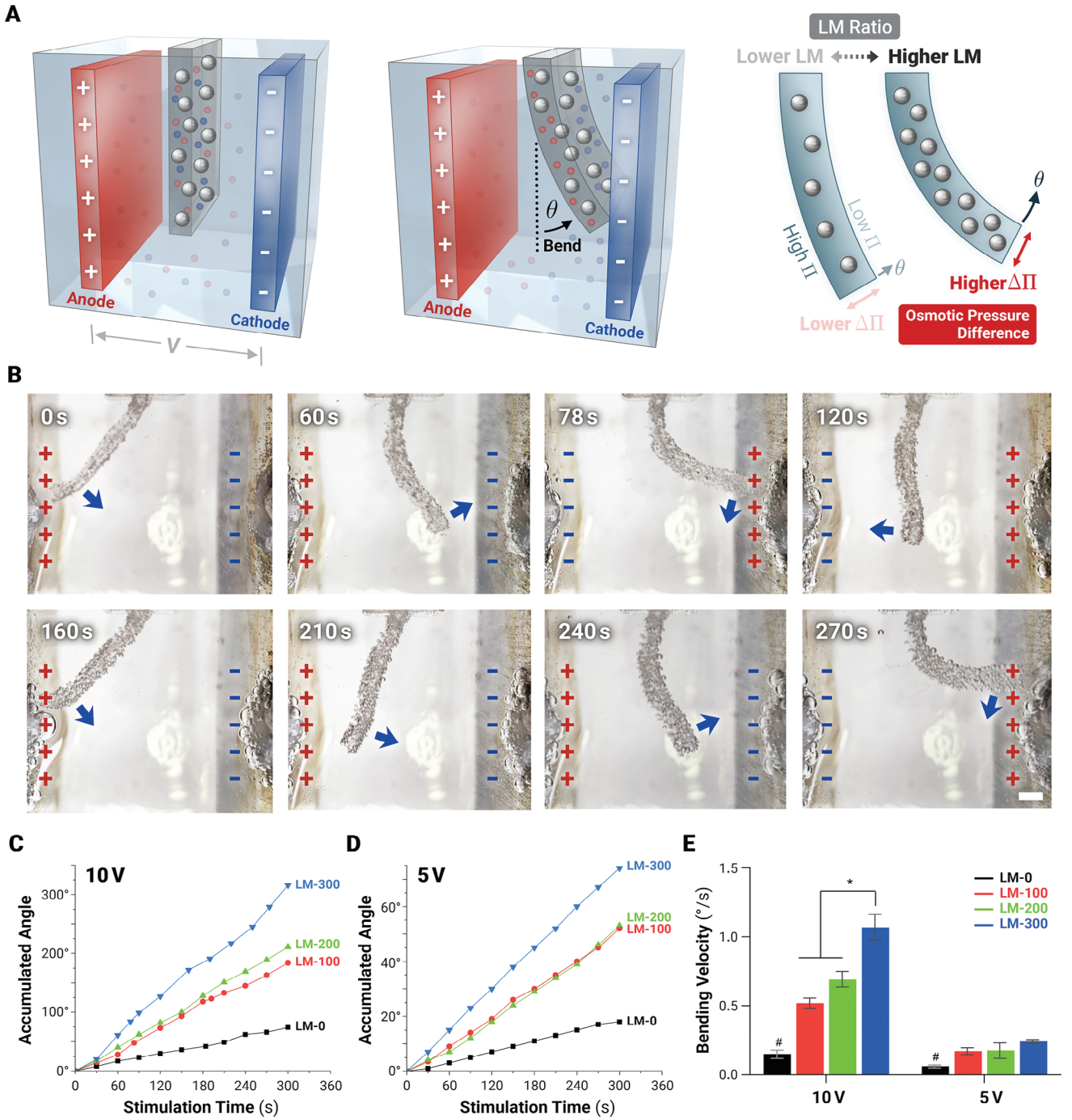


Figure 5. Effects of LM microdroplets on ionic mobility in hydrogels as bending actuators. A) Left: The LM-embedded hydrogel is submerged in an aqueous electrolytic solution, where the ions freely move in the water within the hydrogel matrix. Right: Schematic of bending behavior, which is the result of an osmotic pressure difference ΔΠ across the LM-hydrogel film. It is theorized that higher LM ratios result in higher ΔΠ. B) Actual image of bending hydrogel for the LM-300 group after applying a voltage of 10 V for 270 s, scale bar 3 mm. C,D) Accumulation bending angle due to electric field stimuli ($|E| = 10$, 5 V) for 300 s. E) Bending velocity increases with LM content. $^{*}p < 0.05$, $^{\#}p < 0.05$ LM-hydrogel groups compared to the LM-0 group at the same voltage.

and osmotic pressure. We derived that the osmotic pressure difference ΔΠ is approximately proportional to c^{-} (immobile anion concentration) and $(h^{+})^{2}$ (h^{+}: rate of cation transport). A geometric calculation further reveals that bending speed ($d\theta/dt$) increases when there are more immobile anions (i.e., higher c^{-}) and stronger stimuli (i.e., higher field strength E). By this analysis, we hypothesize that the bending performance of the proposed LM-hydrogel actuators can be enhanced with higher LM ratios, which increases the osmotic pressure difference across the LM-hydrogel (Figure 5A).

© 2023 The Authors. Advanced Functional Materials published by Wiley-VCH GmbH

16163028, 0, Downloaded from https://onlinelibrary.wiley.com/doi/10.1002/adfm.202308238 by Koc University, Wiley Online Library on [26/02/2024]. See the Terms and Conditions (https://onlinelibrary.wiley.com/terms-and-conditions) on Wiley Online Library for rules of use; OA articles are governed by the applicable Creative Commons License

16163028, 0, Downloaded from https://onlinelibrary.wiley.com/doi/10.1002/adfm.202308238 by Koc University, Wiley Online Library on [26/02/2024]. See the Terms and Conditions (https://onlinelibrary.wiley.com/terms-and-conditions) on Wiley Online Library for rules of use; OA articles are governed by the applicable Creative Commons License

2.4.2. Electrical Bending Actuators

To demonstrate the effect of LM microdroplets in ionic actuation of hydrogels, we prepared LM-hydrogel thin films (length: 2 cm, depth: 1 cm, thickness: 1 mm) with different LM contents (0, 100, 200, and 300 mg) and tested each sample by anchoring it on one end in an electrolytic solution (phosphate-buffered saline, PBS) where a voltage (5 and 10 V) is applied across the hydrogel at a distance of $d = 3$ cm. Video analysis (Figure 5B; Video S3, Supporting Information) shows that all samples bend toward the cathode under the electric field, with the higher voltage (10 V) inducing larger bending angles than the lower voltage (5 V) regardless of LM contents (Figure 5C,D). LM-hydrogel actuators with higher LM ratios display higher average bending velocities (Figure 5E) with both $E = 5$ V and 10 V, which confirms that LM inclusion, likely through increasing the osmotic pressure difference, enhances actuation speed. Compared to similar work on bending hydrogel actuators (Figure 1B), our LM-hydrogels are more electrically responsive, with tunable responsiveness by LM ratios.

The role of LM microdroplets in bending enhancement is theorized by two possible mechanisms (Section S2, Supporting Information), where the primary pathway is related to the asymmetric osmotic pressure as a result of immobilized anions COO^- in the LM-hydrogel matrix. In this hypothesis, higher LM ratios are linked to more Ga^{3+} ions released during sonication and hence a higher degree of ionization of the anions COO^-, rather than other cations. When an electric potential is applied, cations drift at a velocity $v_{drift} \propto E$, which has an additional influence on $\Delta\Pi$ (Equations (S3), (S11) in Section S2, Supporting Information). Another likely mechanism is the local acceleration of cations due to the surface charges on the LM microdroplets. As ions naturally form an electric double layer (EDL) on the LM surfaces, it is theorized that a cation will see additional Coulomb forces as it travels through the LM-hydrogel, thereby increasing the v_{drift} further. Further investigations are necessary to analyze these proposed roles of LM. Overall, we showed the physical effects of LM microdroplets on hydrogels as bending actuators by influencing ion mobility and hence the osmotic pressure difference. In the context of ionic bending hydrogels, this work features the use of LM inclusion that enhances actuation both by likely dual mechanisms of ionic crosslinks and interfacial properties.

2.4.3. Robot Locomotion by Asymmetric Bending

The functionality of the electrically responsive ionic LM-hydrogel is not limited to the anchored motion, where one end of the hydrogel film is fixed while force is output at the free moving.[86] Although this operation mode is commonly demonstrated for limited applications with low frequency oscillations, we emphasize that the advantage of such LM-enhanced hydrogels can be taken for whole-body locomotion of a soft robot. Similar to typical locomotion strategies in biological and soft robotics systems,[87] a robot can be designed to produce crawling-like or walking-like gait patterns by having some limbs in frictional contact with a surface while allowing other limbs to move freely.[23,88,89] To demonstrate this, we built a two-limb robot by connecting two rectangular strips of LM-hydrogel (length: 20 mm, depth: 3 mm, thickness: 2.5 mm) with two different LM contents (LM-100 and LM-300) assisted by their self-healing tendency (Figure 6 A–C). We placed the robot in a customized channel (cross-sectional height: 8 mm, depth: 3 mm) surrounded by acrylic sheets. Two graphite pencil rods were placed across the channel at a distance of 5 cm, where a voltage of 50 V was applied (**Figures 6**D). Graphite electrodes were selected over metals to prevent corrosion during the experiment since they are relatively more electrochemically inert. The robot was positioned inside the channel such that at least one of the three vertices was in frictional contact with the wall at any given time.

Upon applying the electric field, the two limbs responded to the ion migration at different velocities (Video S4, Supporting Information) as analyzed above. This asymmetry, therefore, created an overall rotation where the two limbs alternately touched the wall. To generate the overall translational movement of the robot, we reversed electrical polarity whenever a limb loses contact with the wall, thereby allowing the opposite limb to take over (Figure 6 E–H). This locomotion design allows the robot to complete a gait cycle at an overall moving distance of 10.6 mm in 27 s. Here we highlight the advantage of LM inclusion in the hydrogel by ability to modulate the ionic mobility within the hydrogel across different regions in a soft robot body.

2.5. Biocompatibility

The biocompatibility of LM-hydrogel composites (LM-300 and LM-0) was assessed through a co-culture experiment involving four cell lines over one and four days. The cell lines include human mesenchymal stem cells (hMSCs), human fibroblast cells (BJ), NIH mouse fibroblast cells (3T3), and mouse myoblast cells (C2C12). Cell morphology was evaluated using a Live/Dead kit, while cell viability was determined via a CCK-8 assay to calculate the relative growth rate. As shown in **Figure 7**, ≈80% of the cells remained viable, where cell spreading occurred on both the LM-0 and LM-300 surfaces on both days 1 and 4. The inclusion of LM into the PAA-PVA hydrogel network did not inhibit cell proliferation during this period. Remarkable cell growth was observed across all groups from days 1 to 4 at varying rates among different cell lines. On day 1, the cell confluency for all four cell lines was initially low, averaging around 5%. However, by day 4, an increase was observed, especially in the case of BJ cells ($29.29 \pm 4.51\%$) and 3T3 cells ($27.95 \pm 3.78\%$).

These biocompatibility assessment results are consistent with previous studies on cytotoxicity of liquid metal-embedded elastomers to C2C12 cells.[90] In our study, we embedded liquid metal droplets into the hydrogel, where the liquid metal volume is less than 5 vol%. High cell viability and growth are observed across all the cell lines of interest. The cell confluency is low compared to previous studies, which can be explained by the human plasma-derived fibronectin coating on the elastomer, which may promote cell attachment and proliferation. We note that cell interactions may vary between the cell lines and that further investigation is needed to clarify the underlying mechanisms. In summary, the results here show promising potential of the LM-hydrogel composites as an good candidate in biomedical and biohybrid applications where direct contact is needed between the LM-hydrogels and biological cells and tissues.

© 2023 The Authors. Advanced Functional Materials published by Wiley-VCH GmbH

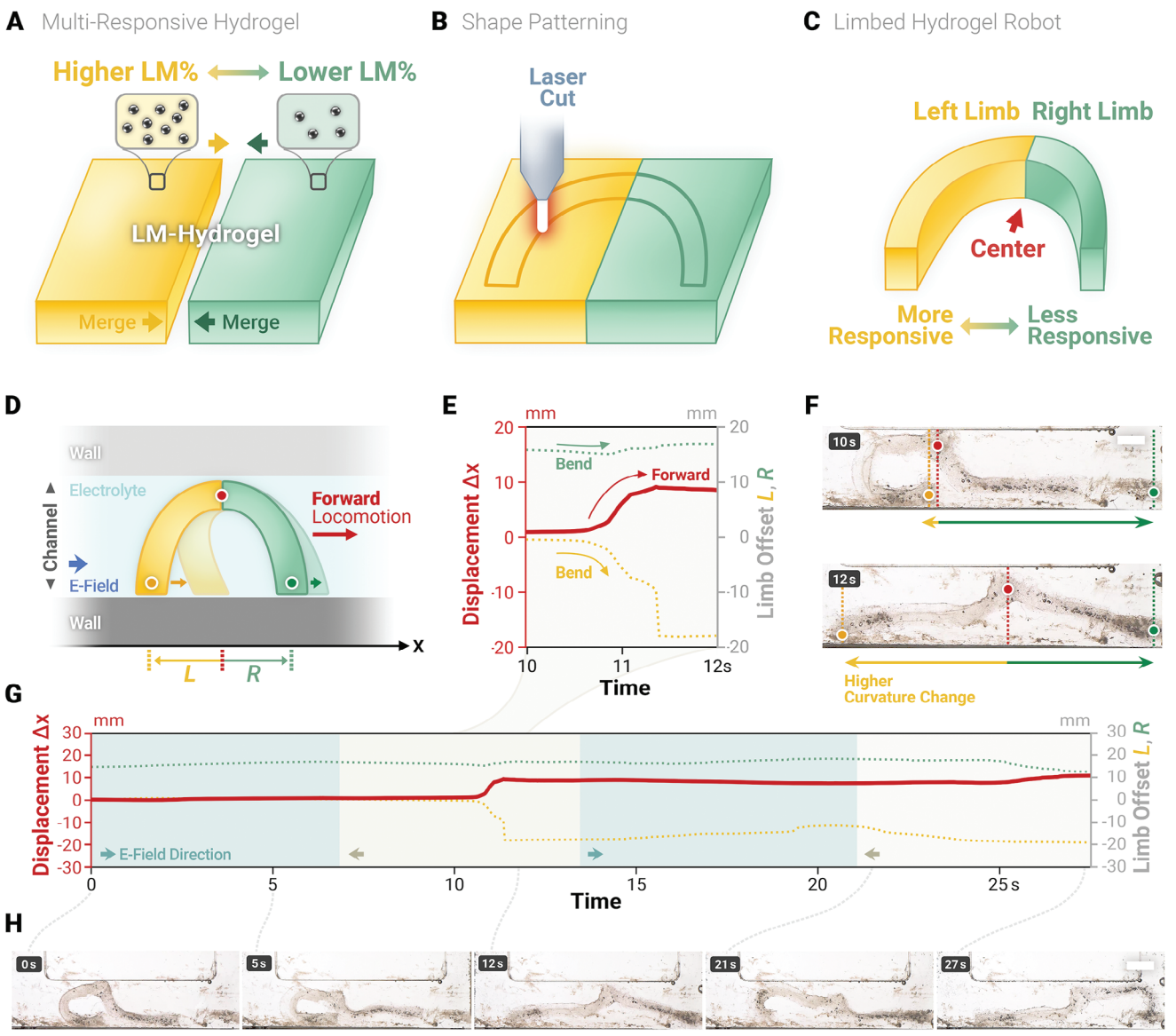


Figure 6. Locomotion of a limbed LM-hydrogel soft robot in a small channel using asymmetric ionic actuation. A) A hydrogel with locally programmable ionic responsivity to an electric field is created by healing two LM-hydrogel sheets in various LM ratios. B) U-shaped robots are laser-cut from the merged hydrogels. C) The limbed robot consists of a higher-LM%, more responsive left limb, and a lower-LM%, less responsive right limb. D) Principles of locomotion of the robot inside a small channel filled with an electrolyte. The robot moves forward through the asymmetric motions between the two limbs. E–H) Gait analysis of the robot with periodically reversed electric fields. With a higher curvature change in the more responsive left limb compared to the right limb (F), the robot center moves forward by 10.6 mm as a result. This process can be repeated for periodic gait cycles.

3. Conclusion

This work contributes to the field of composite hydrogels by introducing a LM-PAA-PVA composite where LM microdroplets have dual roles as a polymerization initiator and as passive inclusion that influences the stimuli-responsive behaviors of the LM-hydrogel. As an initiator for polymerization, LM microdroplets provide radicals due to the atomic configuration of Ga and ionic crosslinks with the ionized Ga^{3+}. The various free radical sources, crosslinking bonds, and higher viscosity of the AA-PVA solution altogether contribute to an ultra-fast polymerization time (≈1 min compared to several hours by conventional polymerization methods). The resulting hydrogel demonstrates a dynamic transition from a soft to a tough and ultimately rigid stage, each displaying distinctive characteristic mechanical properties. As a stimuli-responsive material, the effects of LM microdroplets polymerization and inclusion on the mechanical behaviors of the hydrogel are examined with two different types of stimuli. First, we analyze the swelling behavior in the LM-hydrogels as influenced nonlinearly by LM ratios. It is theorized in this work that the macroscopic capability to absorb water into the porous hydrogel structure is the net result of the dual roles of LM as polymerization initiator and passive inclusion. To demonstrate the structural benefit of this LM-controlled hydrogel architecture,

© 2023 The Authors. Advanced Functional Materials published by Wiley-VCH GmbH

16163028, 0, Downloaded from https://onlinelibrary.wiley.com/doi/10.1002/adfm.202308238 by Koc University, Wiley Online Library on [26/02/2024]. See the Terms and Conditions (https://onlinelibrary.wiley.com/terms-and-conditions) on Wiley Online Library for rules of use; OA articles are governed by the applicable Creative Commons License

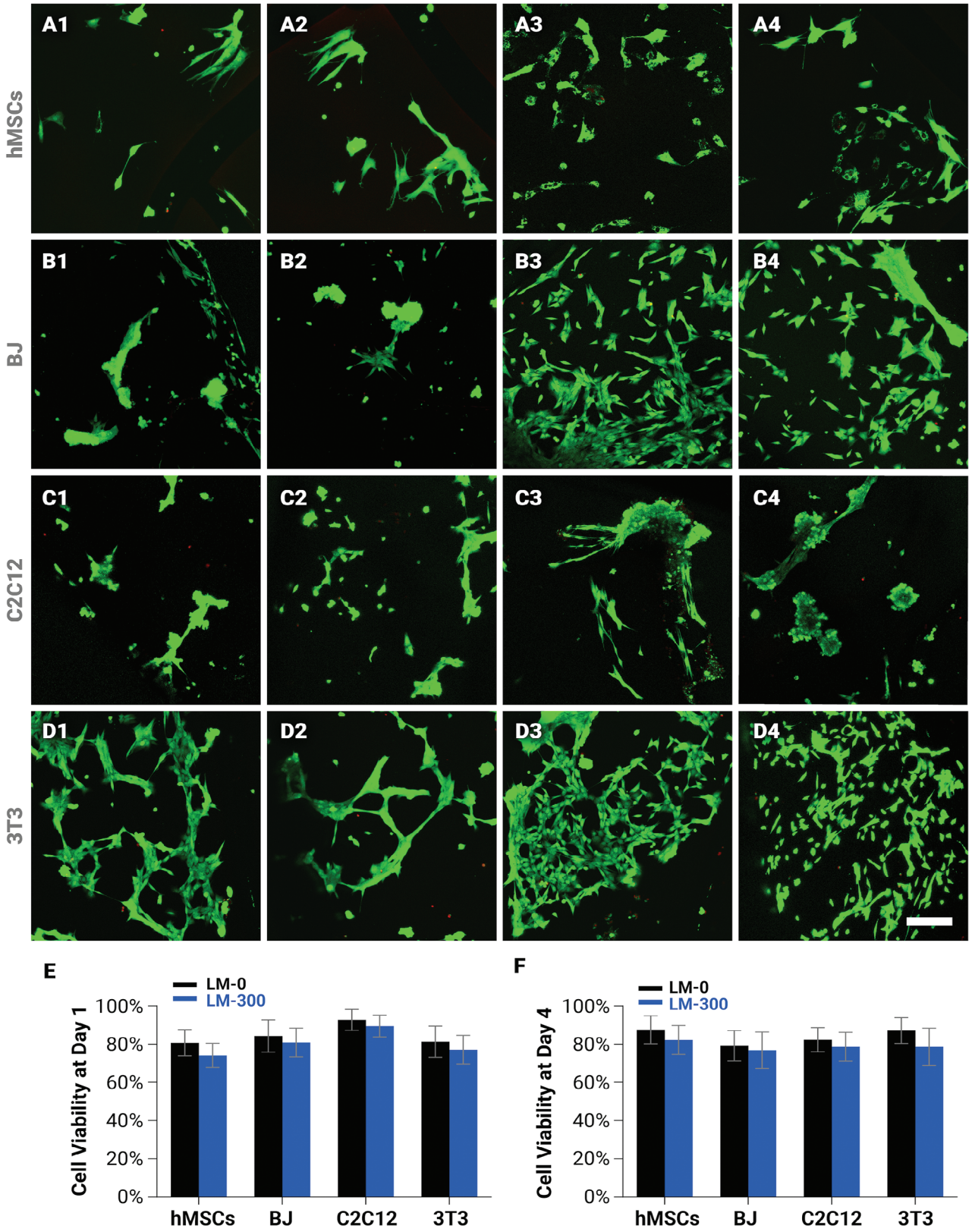


Figure 7. Biocompatibility of the LM-hydrogel composites after swelling. Live/dead cell images in the LM-0 (A1–D1, A3–D3) and LM-300 (A2–D2, A4–D4) groups at day 1 (A1–D1, A2–D2) and day 4 (A3–D3, A4–D4). Different cell lines (hMSCs: A1–A4, BJ: B1–B4, C2C12: C1–C4, 3T3: D1–D4) were co-cultured with LM-hydrogel composite, scale bar: 20 µm. E) Quantitative analysis of cell viability on day 1 (E) and day 4 (F).

© 2023 The Authors. Advanced Functional Materials published by Wiley-VCH GmbH

16163028, 0, Downloaded from https://onlinelibrary.wiley.com/doi/10.1002/adfm.202308238 by Koc University, Wiley Online Library on [26/02/2024]. See the Terms and Conditions (https://onlinelibrary.wiley.com/terms-and-conditions) on Wiley Online Library for rules of use; OA articles are governed by the applicable Creative Commons License

16163028, 0, Downloaded from https://onlinelibrary.wiley.com/doi/10.1002/adfm.202308238 by Koc University, Wiley Online Library on [26/02/2024]. See the Terms and Conditions (https://onlinelibrary.wiley.com/terms-and-conditions) on Wiley Online Library for rules of use; OA articles are governed by the applicable Creative Commons License

we demonstrate a self-folding functionality by asymmetrically swelling the LM-hydrogels in different LM microdroplets ratios. Furthermore, the swollen rigid LM-hydrogels exhibit remarkable stretchability that is ≈10 times higher than that of the LM-free, UV-crosslinked PAA-PVA hydrogels. Second, we study the bending behavior of the LM-hydrogels due to their osmotic pressure differences under an electric field. These electrically responsive actuators are theorized to bend faster with higher LM contents as they create higher ionization of the COO^- cations, which further increases the osmotic pressure difference. The experimental results of ionically actuating the LM-hydrogels agree with the theoretical models. We demonstrate that this LM-controlled ionic actuation of hydrogels can be applied to robot locomotion. Toward potential biomedical applications, the LM-hydrogel shows biocompatibility with co-cultured hMSCs, BJ, 3T3, and C2C12 cells.

Overall, this work shows the functional benefits of the ultrafast polymerization of hydrogels using LM microdroplets as the initiator, which goes beyond conventional hydrogel polymerization techniques. This progress in using LM microdroplets for their dual roles in hydrogels shows particular advantages in stimuli-responsive hydrogels. Future investigations into fundamental principles of the dual or multiple roles of LM in a hydrogel system, as well as their physical effects on hydrogel behaviors such as swelling and osmosis, will inform further enhancement of the proposed LM-hydrogel. Finally, further development of multifunctionalities enabled by LM-polymerized hydrogels will benefit further robotic and biomedical applications and open up new opportunities in this unconventional class of composites.

4. Experimental Section

Materials: The liquid metal (LM, 75% Ga and 25% In) was fabricated by mixing raw gallium (Fischer Scientific 11381238) and indium (Fischer Scientific 11377028) at 195 °C overnight. Acrylic acid, polyvinyl alcohol ($M_w \approx$ 80,000–120,000), phosphate-buffered saline (PBS), glutaraldehyde solution, ethylene glycol dimethacrylate, and 2,2-dimethoxy-2-phenylacetophenone were purchased from Sigma-Aldrich.

Synthesis of LMs-PAA-PVA Composite Hydrogel and Pure PAA-PVA Hydrogel: Poly(vinyl alcohol) (0.65 g) and acrylic acid (6.85 mL) were dissolved in 6.5 mL of PBS solution. The mixtures were stirred on a magnetic stirrer at 130 °C for 3 h to achieve homogeneity and complete polymer dissolution. To form the soft LM-200 hydrogel, 200 mg (2.7 wt%) of liquid metal was added to half of the above solution, followed by ultrasonication (500 W, 20 kHz, 40% amplitude, pulse on 3 s, pulse off 1 s, Fisherbrand) for 1 min in a water bath. The resulting LM soft hydrogel was transferred onto a non-stick plate, and another non-stick plate was placed on top, with a 1 mm gap between them. A weight of 10 kg was applied to ensure a flat and uniform surface of the hydrogel. For the pure PAA-PVA hydrogel, glutaraldehyde solution (81.2 µL, 25% in DI water), ethylene glycol dimethacrylate (200 µL, 98%), and 2,2-dimethoxy-2-phenylacetophenone (0.15 wt%, 99%) were dissolved in dimethyl sulfoxide (99.9%) solution (300 µL), which served as an initiator for polymerization. The initiating agent was added to the AA-PVA solution, and the polymerization solution was poured into PET mold frames with predefined thicknesses (1000 µm). The mold-confined solutions were polymerized by UV light irradiation (365 nm, 30 W) for 30 min. Based on the different amounts of liquid metal (0 mg (0 wt%), 100 mg (1.3 wt%), 200 mg (2.7 wt%), and 300 mg (4 wt%)) mixed with the AA-PVA solution, the groups were labeled as follows: LM-0, LM-100, LM-200, and LM-300.

Instrumental Characterization: Tensile test samples were prepared using the TSC ISO 527-2-5B Dog Bone standard size (35 mm × 6 mm) using test sample cutters. These samples were then tested on a materials testing system (Instron 5942, Illinois Tool Works Inc.) equipped with a 50 N load cell and an extension rate of 0.5 mm s^{-1}. The distribution of LMs, as well as the surface and cross-section morphology of both the rigid hydrogel and the freeze-dried swelling hydrogel, were observed using a field emission scanning electron microscope (SEM 1530VP, Zeiss). Prior to observation, the samples were coated with a thin layer of gold. To visualize the distribution of LMs particles in the hydrogel network, a confocal microscope (SP8, Leica) was employed. Viscosity, shear stress, and oscillatory shear rheology measurements were conducted using a TA Instruments Discovery HR-2 rheometer with a 25 mm parallel plate and a 0.5 mm gap distance, maintained at a temperature of 25 °C. Strain sweeps were performed at variable strain levels ranging from 0.1% to 100% at an oscillation frequency of 6.28 rad s^{-1}. Frequency sweeps were performed at a constant strain of 2.5% and oscillation frequencies ranging from 0.1 to 100 rad s^{-1}. The hydrogel structure was analyzed using Fourier transform infrared (FTIR) spectroscopy (Bruker TENSOR II). The surface properties of the rigid hydrogel were measured using an optical contact angle goniometer (OCA25, DataPhysics Instruments).

Methods for Self-Healing: The dog-bone hydrogel sample was cut into two identical pieces with a knife and the two pieces were immediately brought into contact with each other by manual pressure to promote healing at the interface. The stress–strain curves of the healed samples were obtained through mechanical testing. The self-healing efficiency was calculated by comparing the breaking elongation of the healed samples to that of the original samples and expressing it as a ratio.

Methods for Swelling: The swelling behavior of the rigid LM composite hydrogel was evaluated by monitoring the weight of the hydrogels over time. The hydrogels ($n = 3$) were immersed in 2 mL of deionized water at room temperature. The weight of the hydrogels was measured at regular intervals: every 10 min in the first hour, every 20 min in the first 4 h, and then daily until 1 week. Before weighing each swollen hydrogel sample, it was withdrawn from the deionized water and quickly blotted with absorbent paper to remove excess water. The swelling ratio (Q) was calculated using the following formula: $Q = (m_t/m_0) \times 100\%$, where m_0 represents the initial weight of the hydrogel at $t = 0$ h, and m_t represents the weight of the hydrogel at time t. For the fabrication of the soft robot, two small pieces of rigid plastic sheets were aligned with the rigid LM hydrogel in the length direction. They were then attached together with a piece of 3M Scotch tape to assemble the sample. Next, a water droplet of 50 µL was pipetted onto the surface of the rigid LM composite hydrogel, and the shape change was recorded on a camera.

Methods for Ionic Actuation: To investigate the bending behavior of the rigid LM composite hydrogels, a swelling process was conducted for 4 h by immersing the hydrogel in water. A hydrogel strip was prepared, with one end fixed horizontally, and it was placed in a transparent chamber filled with PBS solution. The chamber contained two aluminum electrodes positioned 60 mm apart. To induce bending in the hydrogel strip, a voltage was applied between the two electrodes using an RS PRO digital laboratory power supply. The bending of the hydrogel strip was recorded on a phone camera. The bending angle of the hydrogel was measured by comparing its deviation from the neutral angular position. For the fabrication of the multi-material soft robot, the LM-100, and LM-300 soft composite hydrogels were joined together to create a multi-material tough hydrogel. The soft robot was then cut to ensure that one limb consisted of the LM-100 material, while the other limb consisted of the LM-300 material. After undergoing the same swelling process, a voltage of 50 V was applied to two graphite electrodes to induce locomotion.

Cytotoxicity Characterization: The biocompatibility of the LM composite hydrogels was evaluated using human mesenchymal stem cells (hMSCs), human fibroblast cells (BJ), NIH mouse fibroblast cells (3T3), and mouse myoblast cells (C2C12) and two different assays: the LIVE/DEAD Cell Imaging Kit and the Cell Counting Kit-8 assay (CCK-8). First, the rigid hydrogel samples (LM-0 and LM-300) were sterilized using UV light for 1 h. Then, they were fully immersed in a cell culture medium (DMEM, 10% FBS, 1% Penicillin-Streptomycin) and kept in an incubator at 37 °C with 5% CO_2 for 7 days, with daily medium changes. Meanwhile, hMSCs, BJ, C2C12, and 3T3 cells were cultured in a T75 flask until they reached 80% confluency. The LM hydrogel samples were added to the cell culture at a density of 5×10^5 cells per well, and the medium was changed every 2 days.

© 2023 The Authors. Advanced Functional Materials published by Wiley-VCH GmbH

On days 1 and 4, a 10% CCK-8 solution was added to the cultures, which were incubated for 1 h. The absorbance of the samples was then measured at 460 nm using a plate reader (BioTek's Synergy H1, Winooski). The cell viability was expressed by the relative growth rate, which was calculated by cell viability = $(OD_{sample}/OD_{blank}) \times 100\%$, where OD_{sample} is the optical density of the LM-hydrogel sample (LM-300) and the control sample (LM-0). OD_{blank} is the optical density of the blank control. For assessing cell morphology, the LIVE/DEAD Cell imaging kit was used after 1 and 4 days of culture. Confocal microscopy (SP8, Leica) was used to visualize both live and dead cells and capture three representative images of each scaffold at a magnification of 10×. Cell confluency, defined as the percentage of the cell culture material area covered by adherent cells, was calculated using ImageJ by dividing the cell area by the total area.

Statistical Analysis: All data were expressed as mean ± standard deviation (SD), with $n = 3$ per group. GraphPad Prism 8 (GraphPad, California, USA) was used to perform the statistical analysis of the obtained data and $^*p < 0.05$ was considered statistically significant.

Supporting Information

Supporting Information is available from the Wiley Online Library or from the author.

Acknowledgements

J.Z. and J.L. contributed equally to this work. This work was funded by the Max Planck Society and the European Research Council (ERC) Advanced Grant SoMMoR project with grant no. 834531. J.Z. gratefully acknowledges the support from the Max Planck Queensland Center for the Materials Science of Extracellular Matrices.

Open access funding enabled and organized by Projekt DEAL.

Conflict of Interest

The authors declare no conflict of interest.

Data Availability Statement

The data that support the findings of this study are available from the corresponding author upon reasonable request.

Keywords

hydrogel polymerization, liquid metal, soft robotics, stimuli-responsive

Received: July 17, 2023
Revised: October 5, 2023
Published online:

[1] J.-Y. Sun, X. Zhao, W. R. Illeperuma, O. Chaudhuri, K. H. Oh, D. J. Mooney, J. J. Vlassak, Z. Suo, *Nature* **2012**, *489*, 133.
[2] Y. Ohm, C. Pan, M. J. Ford, X. Huang, J. Liao, C. Majidi, *Nat. Electron.* **2021**, *4*, 185.
[3] Y. Zhou, C. Wan, Y. Yang, H. Yang, S. Wang, Z. Dai, K. Ji, H. Jiang, X. Chen, Y. Long, *Adv. Funct. Mater.* **2019**, *29*, 1806220.
[4] X. Wang, P. Wu, *ACS Appl. Mater. Interfaces* **2018**, *10*, 2504.
[5] H. Yuk, S. Lin, C. Ma, M. Takaffoli, N. X. Fang, X. Zhao, *Nat. Commun.* **2017**, *8*, 14230.
[6] C. Keplinger, J.-Y. Sun, C. C. Foo, P. Rothemund, G. M. Whitesides, Z. Suo, *Science* **2013**, *341*, 984.
[7] H. Na, Y.-W. Kang, C. S. Park, S. Jung, H.-Y. Kim, J.-Y. Sun, *Science* **2022**, *376*, 301.
[8] D. Liu, L. Su, J. Liao, B. Reeja-Jayan, C. Majidi, *Adv. Energy Mater.* **2019**, *9*, 1902798.
[9] T. B. Schroeder, A. Guha, A. Lamoureux, G. VanRenterghem, D. Sept, M. Shtein, J. Yang, M. Mayer, *Nature* **2017**, *552*, 214.
[10] Z. Wang, H. Li, Z. Tang, Z. Liu, Z. Ruan, L. Ma, Q. Yang, D. Wang, C. Zhi, *Adv. Funct. Mater.* **2018**, *28*, 1804560.
[11] L. Shuai, Z. H. Guo, P. Zhang, J. Wan, X. Pu, Z. L. Wang, *Nano Energy* **2020**, *78*, 105389.
[12] J. Kang, J. B.-H. Tok, Z. Bao, *Nat. Electron.* **2019**, *2*, 144.
[13] Y. Zhao, Y. Ohm, J. Liao, Y. Luo, H.-Y. Cheng, P. Won, P. Roberts, M. R. Carneiro, M. F. Islam, J. H. Ahn, L. M. Walker, C. Majidi, *Nat. Electron.* **2023**, *6*, 206.
[14] C. Yu, Z. Duan, P. Yuan, Y. Li, Y. Su, X. Zhang, Y. Pan, L. L. Dai, R. G. Nuzzo, Y. Huang, H. Jiang, J. A. Rogers, *Adv. Mater.* **2013**, *25*, 1541.
[15] X. Liu, J. Liu, S. Lin, X. Zhao, *Mater. Today* **2020**, *36*, 102.
[16] M. J. Ford, Y. Ohm, K. Chin, C. Majidi, *J. Mater. Res.* **2022**, *37*, 2.
[17] H. Yuk, J. Wu, X. Zhao, *Nat. Rev. Mater.* **2022**, *7*, 935.
[18] J. Zhang, H. Eyisoylu, X.-H. Qin, M. Rubert, R. Müller, *Acta Biomater.* **2021**, *121*, 637.
[19] S. R. Shin, S. M. Jung, M. Zalabany, K. Kim, P. Zorlutuna, S. b. Kim, M. Nikkhah, M. Khabiry, M. Azize, J. Kong, K.-T. Wan, T. Palacios, M. R. Dokmeci, H. Bae, X. Tang, A. Khademhosseini, *ACS Nano* **2013**, *7*, 2369.
[20] Y. Ahn, H. Lee, D. Lee, Y. Lee, *ACS Appl. Mater. Interfaces* **2014**, *6*, 18401.
[21] S. R. Goudu, I. C. Yasa, X. Hu, H. Ceylan, W. Hu, M. Sitti, *Adv. Funct. Mater.* **2020**, *30*, 2004975.
[22] H. Ceylan, N. O. Dogan, I. C. Yasa, M. N. Musaoglu, Z. U. Kulali, M. Sitti, *Sci. Adv.* **2021**, *7*, eabh0273.
[23] Y. Ohm, J. Liao, Y. Luo, M. J. Ford, C. Majidi, *Adv. Mater.* **2023**, *35*, 2209408.
[24] P. Thoniyot, M. J. Tan, A. A. Karim, D. J. Young, X. J. Loh, *Adv. Sci.* **2015**, *2*, 1400010.
[25] C. Majidi, *Matter* **2021**, *4*, 336.
[26] M. D. Dickey, R. C. Chiechi, R. J. Larsen, E. A. Weiss, D. A. Weitz, G. M. Whitesides, *Adv. Funct. Mater.* **2008**, *18*, 1097.
[27] J. Liao, C. Majidi, *Adv. Sci.* **2022**, *9*, 2201963.
[28] J. Liao, C. Majidi, M. Sitti, *Adv. Mater.* **2023**, 2300560.
[29] J.-H. Kim, S. Kim, J.-H. So, K. Kim, H.-J. Koo, *ACS Appl. Mater. Interfaces* **2018**, *10*, 17448.
[30] M. D. Bartlett, A. Fassler, N. Kazem, E. J. Markvicka, P. Mandal, C. Majidi, *Adv. Mater.* **2016**, *28*, 3726.
[31] M. D. Bartlett, N. Kazem, M. J. Powell-Palm, X. Huang, W. Sun, J. A. Malen, C. Majidi, *Proc. Natl. Acad. Sci. U. S. A.* **2017**, *114*, 2143.
[32] N. Kazem, M. D. Bartlett, C. Majidi, *Adv. Mater.* **2018**, *30*, 1706594.
[33] D. L. Taylor, M. in het Panhuis, *Adv. Mater.* **2016**, *28*, 9060.
[34] T. Shay, O. D. Velev, M. D. Dickey, *Soft Matter* **2018**, *14*, 3296.
[35] Y. Yu, F. Liu, R. Zhang, J. Liu, *Adv. Mater. Technol.* **2017**, *2*, 1700173.
[36] J. Ma, Y. Lin, Y.-W. Kim, Y. Ko, J. Kim, K. H. Oh, J.-Y. Sun, C. B. Gorman, M. A. Voinov, A. I. Smirnov, J. Genzer, M. D. Dickey, *ACS Macro Lett.* **2019**, *8*, 1522.
[37] J. Xu, Z. Wang, J. You, X. Li, M. Li, X. Wu, C. Li, *Chem. Eng. J.* **2020**, *392*, 123788.
[38] Q. Wang, C. Pan, Y. Zhang, L. Peng, Z. Chen, C. Majidi, L. Jiang, *Matter* **2023**, *6*, 855.
[39] H. Wang, S. Chen, X. Zhu, B. Yuan, X. Sun, J. Zhang, X. Yang, Y. Wei, J. Liu, *Matter* **2022**, *5*, 2054.
[40] K. B. Ozutemiz, J. Wissman, O. B. Ozdoganlar, C. Majidi, *Adv. Mater. Interfaces* **2018**, *5*, 1701596.

© 2023 The Authors. Advanced Functional Materials published by Wiley-VCH GmbH

16163028, 0, Downloaded from https://onlinelibrary.wiley.com/doi/10.1002/adfm.202308238 by Koc University, Wiley Online Library on [26/02/2024]. See the Terms and Conditions (https://onlinelibrary.wiley.com/terms-and-conditions) on Wiley Online Library for rules of use; OA articles are governed by the applicable Creative Commons License

[41] J. Ma, F. Krisnadi, M. H. Vong, M. Kong, O. M. Awartani, M. D. Dickey, *Adv. Mater.* **2022**, *35*, 2205196.
[42] J. Liao, C. Majidi, *Soft Matter* **2021**, *17*, 1921.
[43] V. Vallem, E. Roosa, T. Ledinh, W. Jung, T.-i. Kim, S. Rashid-Nadimi, A. Kiani, M. D. Dickey, *Adv. Mater.* **2021**, *33*, 2103142.
[44] Z. Tai, J. Yang, Y. Qi, X. Yan, Q. Xue, *RSC Adv.* **2013**, *3*, 12751.
[45] N. Zhang, R. Li, L. Zhang, H. Chen, W. Wang, Y. Liu, T. Wu, X. Wang, W. Wang, Y. Li, Y. Zhaoa, J. Gao, *Soft Matter* **2011**, *7*, 7231.
[46] G. M. Milani, I. T. Coutinho, F. N. Ambrosio, M. H. Monteiro do Nascimento, C. B. Lombello, E. C. Venancio, M. Champeau, *J. Appl. Polym. Sci.* **2022**, *139*, 52091.
[47] J. Fei, Z. Zhang, L. Gu, *Polym. Int.* **2002**, *51*, 502.
[48] S. Y. Kim, H. S. Shin, Y. M. Lee, C. N. Jeong, *J. Appl. Polym. Sci.* **1999**, *73*, 1675.
[49] K. Qiao, S. Guo, Y. Zheng, X. Xu, H. Meng, J. Peng, Z. Fang, Y. Xie, *Mater. Sci. Eng., C* **2018**, *93*, 853.
[50] Y. Li, Y. Sun, Y. Xiao, G. Gao, S. Liu, J. Zhang, J. Fu, *ACS Appl. Mater. Interfaces* **2016**, *8*, 26326.
[51] H. Jiang, L. Fan, S. Yan, F. Li, H. Li, J. Tang, *Nanoscale* **2019**, *11*, 2231.
[52] H. L. Lim, J. C. Chuang, T. Tran, A. Aung, G. Arya, S. Varghese, *Adv. Funct. Mater.* **2011**, *21*, 55.
[53] Y. Wang, N. Alizadeh, M. Barde, M. L. Auad, B. S. Beckingham, *ACS Appl. Polym. Mater.* **2022**, *4*, 971.
[54] Y. Shin, M.-Y. Choi, J. Choi, J.-H. Na, S. Y. Kim, *ACS Appl. Mater. Interfaces* **2021**, *13*, 15633.
[55] S. Jin, J. Gu, Y. Shi, K. Shao, X. Yu, G. Yue, *Eur. Polym. J.* **2013**, *49*, 1871.
[56] S.-B. Lin, C.-H. Yuan, A.-R. Ke, Y.-L. Li, N. Ouyang, *Adv. Polym. Technol.* **2013**, *32*, E20.
[57] M. Liao, H. Liao, J. Ye, P. Wan, L. Zhang, *ACS Appl. Mater. Interfaces* **2019**, *11*, 47358.
[58] G. H. Robinson, *Acc. Chem. Res.* **1999**, *32*, 773.
[59] Y. Su, J. Zhao, W. Zhan, H. Yuan, L. Wu, G. Sui, H. Zhang, *Chem. Eng. J.* **2022**, *435*, 135018.
[60] M. B. Ghasemian, M. Mayyas, S. A. Idrus-Saidi, M. A. Jamal, J. Yang, S. S. Mofarah, E. Adabifiroozjaei, J. Tang, N. Syed, A. P. O'Mullane, T. Daeneke, K. Kalantar-Zadeh, *Adv. Funct. Mater.* **2019**, *29*, 1901649.
[61] H. U. Moritz, *Chem. Eng. Technol.* **1989**, *12*, 71.
[62] Y. Wen, X. Zhu, D. E. Gauthier, X. An, D. Cheng, Y. Ni, L. Yin, *Cellulose* **2015**, *22*, 2499.
[63] E. J. Markvicka, M. D. Bartlett, X. Huang, C. Majidi, *Nat. Mater.* **2018**, *17*, 618.
[64] M. M. Ozmen, O. Okay, *Polymer* **2005**, *46*, 8119.
[65] R. Foudazi, R. Zowada, I. Manas-Zloczower, D. L. Feke, *Langmuir* **2023**, *39*, 2092.
[66] H. H. Winter, G. Gappert, H. Ito, *Macromolecules* **2002**, *35*, 3325.
[67] M. Morra, E. Occhiello, F. Garbassi, *Adv. Colloid Interface Sci.* **1990**, *32*, 79.
[68] M. R. Khan, C. B. Eaker, E. F. Bowden, M. D. Dickey, *Proc. Natl. Acad. Sci.* **2014**, *111*, 14047.
[69] I. D. Joshipura, K. A. Persson, V. K. Truong, J.-H. Oh, M. Kong, M. H. Vong, C. Ni, M. Alsafatwi, D. P. Parekh, H. Zhao, M. D. Dickey, *Langmuir* **2021**, *37*, 10914.
[70] D. Vesely, *Polymer* **2001**, *42*, 4417.
[71] E. W. Washburn, *Phys. Rev.* **1921**, *17*, 273.
[72] H. Schott, *J. Macromol. Sci., Part B: Phys.* **1992**, *31*, 1.
[73] J. Ha, J. Kim, Y. Jung, G. Yun, D.-N. Kim, H.-Y. Kim, *Sci. Adv.* **2018**, *4*, eaao7051.
[74] Q. Xu, N. Oudalov, Q. Guo, H. M. Jaeger, E. Brown, *Phys. Fluids* **2012**, *24*, 063101.
[75] X. Liu, M. Gao, J. Chen, S. Guo, W. Zhu, L. Bai, W. Zhai, H. Du, H. Wu, C. Yan, Y. Shi, J. Gu, H. J. Qi, K. Zhou, *Adv. Funct. Mater.* **2022**, *32*, 2203323.
[76] D. P. Holmes, M. Roché, T. Sinha, H. A. Stone, *Soft Matter* **2011**, *7*, 5188.
[77] C. Yoon, R. Xiao, J. Park, J. Cha, T. D. Nguyen, D. H. Gracias, *Smart Mater. Struct.* **2014**, *23*, 094008.
[78] K. S. Kwok, Q. Huang, M. Mastrangeli, D. H. Gracias, *Adv. Mater. Interfaces* **2020**, *7*, 1901677.
[79] L. Ionov, *Adv. Funct. Mater.* **2013**, *23*, 4555.
[80] M. Shojaeifard, S. Niroumandi, M. Baghani, *J. Intell. Mater. Syst. Struct.* **2022**, *33*, 2106.
[81] Y. Liu, B. Shaw, M. D. Dickey, J. Genzer, *Sci. Adv.* **2017**, *3*, e1602417.
[82] M. H. Gharahcheshmeh, K. Gleason, *Mater. Today Adv.* **2020**, *8*, 100086.
[83] Y. Bahramzadeh, M. Shahinpoor, *Soft Rob.* **2014**, *1*, 38.
[84] R. Tiwari, E. Garcia, *Smart Mater. Struct.* **2011**, *20*, 083001.
[85] J. Ko, C. Kim, D. Kim, Y. Song, S. Lee, B. Yeom, J. Huh, S. Han, D. Kang, J.-S. Koh, J. Cho, *Sci. Rob.* **2022**, *7*, eabo6463.
[86] L. Hines, K. Petersen, G. Z. Lum, M. Sitti, *Adv. Mater.* **2017**, *29*, 1603483.
[87] M. Calisti, G. Picardi, C. Laschi, *J. R. Soc., Interface* **2017**, *14*, 20170101.
[88] D. Rus, M. T. Tolley, *Nature* **2015**, *521*, 467.
[89] M. Zadan, D. K. Patel, A. P. Sabelhaus, J. Liao, A. Wertz, L. Yao, C. Majidi, *Adv. Mater.* **2022**, *34*, 2200857.
[90] P. Won, S. Coyle, S. H. Ko, D. Quinn, K. J. Hsia, P. LeDuc, C. Majidi, *Adv. Healthcare Mater.* **2023**, *12*, 2202430.

© 2023 The Authors. Advanced Functional Materials published by Wiley-VCH GmbH

16163028, 0, Downloaded from https://onlinelibrary.wiley.com/doi/10.1002/adfm.202308238 by Koc University, Wiley Online Library on [26/02/2024]. See the Terms and Conditions (https://onlinelibrary.wiley.com/terms-and-conditions) on Wiley Online Library for rules of use; OA articles are governed by the applicable Creative Commons License